

Article

Accelerated Degradation of Poly- ϵ -caprolactone Composite Scaffolds for Large Bone Defects

Evangelos Daskalakis ^{1,*}, Mohamed H. Hassan ¹, Abdalla M. Omar ¹, Anil A. Acar ^{2,3,4}, Ali Fallah ^{2,3,4}, Glen Cooper ¹, Andrew Weightman ¹, Gordon Blunn ⁵, Bahattin Koc ^{2,3,4} and Paulo Bartolo ^{1,6,*}

¹ School of Mechanical, Aerospace and Civil Engineering, University of Manchester, Manchester M13 9PL, UK

² Integrated Manufacturing Technologies Research and Application Center, Sabanci University, Tuzla 34956, Istanbul, Turkey

³ SUNUM Nanotechnology Research Center, Sabanci University, Tuzla 34956, Istanbul, Turkey

⁴ Faculty of Engineering and Natural Sciences, Sabanci University, Tuzla 34956, Istanbul, Turkey

⁵ School of Pharmacy and Biomedical Sciences, University of Portsmouth, Portsmouth PO1 2DT, UK

⁶ Singapore Centre for 3D Printing, School of Mechanical and Aerospace Engineering, Nanyang Technological University, Singapore 639798, Singapore

* Correspondence: evangelos.daskalakis@manchester.ac.uk (E.D.); pbartolo@ntu.edu.sg (P.B.)

Abstract: This research investigates the accelerated hydrolytic degradation process of both anatomically designed bone scaffolds with a pore size gradient and a rectangular shape (biomimetically designed scaffolds or bone bricks). The effect of material composition is investigated considering poly- ϵ -caprolactone (PCL) as the main scaffold material, reinforced with ceramics such as hydroxyapatite (HA), β -tricalcium phosphate (TCP) and bioglass at a concentration of 20 wt%. In the case of rectangular scaffolds, the effect of pore size (200 μ m, 300 μ m and 500 μ m) is also investigated. The degradation process (accelerated degradation) was investigated during a period of 5 days in a sodium hydroxide (NaOH) medium. Degraded bone bricks and rectangular scaffolds were measured each day to evaluate the weight loss of the samples, which were also morphologically, thermally, chemically and mechanically assessed. The results show that the PCL/bioglass bone brick scaffolds exhibited faster degradation kinetics in comparison with the PCL, PCL/HA and PCL/TCP bone bricks. Furthermore, the degradation kinetics of rectangular scaffolds increased by increasing the pore size from 500 μ m to 200 μ m. The results also indicate that, for the same material composition, bone bricks degrade slower compared with rectangular scaffolds. The scanning electron microscopy (SEM) images show that the degradation process was faster on the external regions of the bone brick scaffolds (600 μ m pore size) compared with the internal regions (200 μ m pore size). The thermal gravimetric analysis (TGA) results show that the ceramic concentration remained constant throughout the degradation process, while differential scanning calorimetry (DSC) results show that all scaffolds exhibited a reduction in crystallinity (X_c), enthalpy (Δm) and melting temperature (T_m) throughout the degradation process, while the glass transition temperature (T_g) slightly increased. Finally, the compression results show that the mechanical properties decreased during the degradation process, with PCL/bioglass bone bricks and rectangular scaffolds presenting higher mechanical properties with the same design in comparison with the other materials.

Keywords: 3D printing; additive manufacturing; biomaterials; degradation process



Citation: Daskalakis, E.; Hassan, M.H.; Omar, A.M.; Acar, A.A.; Fallah, A.; Cooper, G.; Weightman, A.; Blunn, G.; Koc, B.; Bartolo, P. Accelerated Degradation of Poly- ϵ -caprolactone Composite Scaffolds for Large Bone Defects. *Polymers* **2023**, *15*, 670. <https://doi.org/10.3390/polym15030670>

Academic Editors: Laura Aliotta, Vito Gigante and Andrea Lazzeri

Received: 6 December 2022

Revised: 13 January 2023

Accepted: 21 January 2023

Published: 28 January 2023



Copyright: © 2023 by the authors. Licensee MDPI, Basel, Switzerland. This article is an open access article distributed under the terms and conditions of the Creative Commons Attribution (CC BY) license (<https://creativecommons.org/licenses/by/4.0/>).

1. Introduction

A major concern related to the design of polymer-based bone tissue engineering scaffolds is related to the degradation process and degradation kinetics of these constructs as well as the rate of tissue regeneration. After generating an in vitro cell culture of a scaffold/tissue system, the degree of remodelling and replacement of the biological implant by the native tissue needs to be considered [1–7]. Tissue remodelling is important to obtain

stable mechanical conditions and vascularization at the implantation site [8–15]. Therefore, scaffolds should maintain sufficient structural integrity during the tissue regeneration process, which must be accompanied by a similar scaffold's degradation kinetics [16–20].

In the case of synthetic polymers such as poly- ϵ -caprolactone (PCL), hydrolysis is considered the most important degradation mechanism, which strongly depends on the type of chemical bonds, copolymer composition and wettability properties [21–25]. This degradation mechanism involves the hydrolysis of unstable ester bonds present in the molecular chain of the polymer [26–30]. Moreover, as these polymers are semi-crystalline materials, it has been pointed out that the degradation occurs through a random hydrolytic split of the amorphous regions followed by the gradual degradation of the crystalline regions [31–38]. However, the degradation mechanism depends on multiple factors related to both the material (e.g., crystallinity and molecular weight) and topological (e.g., pore size and pore shape) characteristics of scaffolds, which are not fully understood. Several papers have been published based on rectangular or cylindrical scaffolds, investigating the effect of pore size and pore architecture and material composition [39–47]. However, a comparison of the degradation kinetics of polymer/ceramic scaffolds containing different ceramic materials (e.g., hydroxyapatite (HA), β -tricalcium phosphate (TCP) and bioglass) is still missing.

Despite the significant advances in the field of bone tissue engineering, one of the biggest challenges from a scaffold design point of view is the difficulty in producing structures capable of simultaneously presenting (1) high mechanical strength and (2) proper degradation kinetics.

Through the design of anatomical design scaffolds with gradient pore sizes mimicking the structure of bone (bone bricks), it was possible to achieve mechanical properties suitable for bone engineering applications, which represents a significant step forward in the field [48,49]. This research investigates the accelerated hydrolytic degradation process of bone bricks with different material compositions to fully understand the effects of gradient pore size and material content on the behaviour of bone brick scaffolds. Accelerated degradation was considered as an alternative to the use of phosphate-buffered saline (PBS) or simulated body fluid due to the long-term degradation of PCL (2–3 years) in physiological conditions, providing relevant data on the behaviour of the different considered materials [50]. This allowed us to investigate, for the first time, the behaviour of PCL-based scaffolds reinforced with the most used ceramic materials. Moreover, the degradation kinetics are compared for rectangular scaffolds with different pore sizes and similar material compositions, providing relevant information on the impact of scaffold architecture.

2. Materials and Methods

2.1. Materials

PCL (melting point = 60 °C, glass transition temperature = –60 °C and molecular weight = 50,000 Da; CAPA 6500, Perstorp Caprolactones, Cheshire, UK) was used as received in the form of pellets. Composite blends were prepared using HA (molecular weight = 502.31 g/mol and melting point = 1100 °C; Sigma-Aldrich, St. Louis, MO, USA) in nanopowder shape (<20 nm particle size), TCP (molecular weight = 310.18 g/mol and melting point = 1391 °C; Sigma-Aldrich, St. Louis, MO, USA) in powder shape (ranging between 20 μ m and 30 μ m) and bioglass 45S5 (6 wt% P₂O₅, 45 wt% SiO₂, 24.5 wt% Na₂O and 24.5 wt% CaO; CeraDynamics Ltd., James Kent Group, Stoke, UK) in powder shape (<10 μ m particles size). A melt blending process was used to prepare the blends.

2.2. Bone Bricks and Scaffolds Production

Bone bricks with different material compositions (PCL, PCL containing 20 wt% of HA, PCL containing 20 wt% of TCP, and PCL containing 20 wt% of bioglass), were fabricated using the screw-assisted additive manufacturing 3D Discovery (RegenHU, Villaz-St-Pierre, Switzerland) and a continuous path algorithm based on 38 zig-zag double filaments and 14 spiral filaments (Figure 1). Similar material compositions were considered for the

fabrication of rectangular scaffolds with uniform pore sizes. A total of 3 different pore sizes were considered: 200 μm , 300 μm and 500 μm (Figure 1). The overall dimensions of the bone bricks were 31 mm \times 26.7 mm \times 10 mm. Both bone bricks and rectangular scaffolds were printed using the following processing parameters: 90 $^{\circ}\text{C}$ melting temperature, 20 mm/s deposition velocity and 12 rpm screw rotational velocity. The filaments were extruded using a 0.33 mm diameter needle.

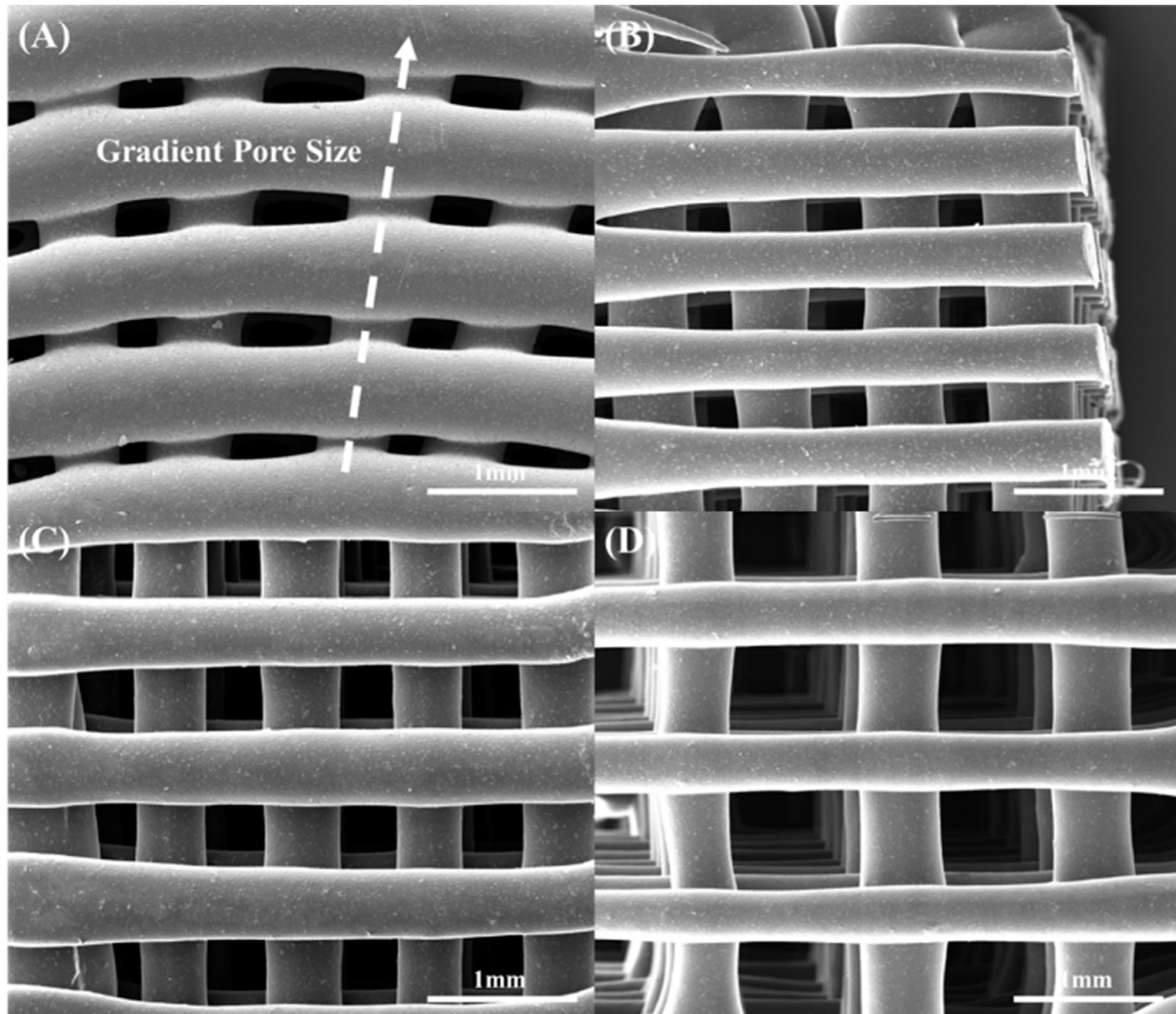


Figure 1. SEM images of (A) bone bricks (PCL/bioglass), (B) 200 μm pore size rectangular scaffolds (PCL/bioglass), (C) 300 μm pore size rectangular scaffolds (PCL/bioglass) and (D) 500 μm pore size rectangular scaffolds (PCL/bioglass).

2.3. Degradation Procedure

Accelerated degradation studies were conducted using sodium hydroxide (NaOH) of 5 mol/L (5 N) in aqueous solution (VWR, Radnor, PA, USA) with a density of 1.185 gr/cm^3 (20 $^{\circ}\text{C}$), a solubility of 20 $^{\circ}\text{C}$ and a pH of 14 (H_2O , 20 $^{\circ}\text{C}$). The degradation period took place for 5 days. On each day, 5 samples were used from each considered case and measured using a high-precision balance. At each time point, the samples were removed from the NaOH and washed three times with the use of deionised water and left to dry overnight. Once completely dry, the samples were measured to determine the weight reduction. The amount of NaOH used for 5 rectangular scaffolds was 15 mL and for the 5 anatomically designed bone bricks, the amount was 50 mL (due to their size). The pH was monitored throughout the experimental work, and no changes were observed (pH of 14).

2.4. Morphological Characterization

Scanning electron microscopy (SEM) was used to investigate the morphological characteristics of the samples and to determine pore sizes (FEI ESEM Quanta 250, FEI Company, Hillsboro, OR, USA). Scaffolds were coated (platinum coating) with the use of an EMITECH K550X sputter coater (Quorum Technologies, Laughton, East Sussex, UK) before imaging. The SEM images were analysed using ImageJ 1.x (National Institutes of Health, Bethesda, MD, USA) (10 measurements per sample).

The porosity of the scaffolds was calculated with the use of the following equation:

$$P_t = \left(\frac{V_p}{V} \right) \times 100 \quad (1)$$

where V_p is the pore volume, V is the total bulk volume and P_t is the porosity.

The density of PCL used in these experiments was calculated as follows:

$$\rho = \frac{m}{V} \quad (2)$$

where ρ is the density of the unprocessed material, m is the mass measured and V is the volume measured. The calculated density of PCL was $1.124 \pm 0.003 \text{ g/cm}^3$.

2.5. Thermal Gravimetric Analysis

Thermal gravimetric analysis, using a TGA Q500 (TA Instruments, New Castle, UK), was used to investigate the thermal degradation and to calculate the ceramic content on the printed scaffolds. Experiments were repeated 4 times per considered scaffold ($n = 4$). The tests were conducted in air atmosphere (50 mL/min) with a temperature ranging from 25 °C to 1000 °C at a rate of 10 °C/min. The weight of each sample was 200 mg, and each test was conducted twice.

2.6. Differential Scanning Calorimetry

Differential scanning calorimetry (DSC) tests were performed to determine the melting temperature (T_m), the enthalpy (ΔH_m), the crystallinity and the glass transition temperature (T_g) ($n = 4$). Tests were conducted using a TA Q100 (TA Instruments, New Castle, UK) under a nitrogen/air atmosphere (50 mL/min). The heating cycle was as follows: heating from -90 °C to 100 °C at a rate of 10 °C/min and then keeping stable for 2 min. The weight of each considered sample was 20 mg.

2.7. Mechanical Testing

Compression tests were performed using an INSTRON 3344 (Instron, High Wycombe, Buckinghamshire, UK) ($n = 4$), at different degradation time points, according to the ASTM D695-15. Force versus displacement curves obtained using the Bluehill Universal Software (Instron, High Wycombe, Buckinghamshire, UK) were stress–strain curves. The compressive modulus was determined based on the slope of the elastic region of the stress–strain curves.

2.8. Data Analysis

Statistical analysis was performed using a one-way analysis of variance (one-way ANOVA) with Tukey's post hoc test (GraphPad Software Inc., San Diego, CA, USA). Weight loss, TGA and DSC data were analysed using Origin 2021 (Origin Lab Corporation, Northampton, MA, USA) and are presented as average values of the obtained results.

3. Results and Discussion

3.1. Degradation Analysis

Figure 2 shows the weight reduction values for the different samples at different degradation time points. The results show that the addition of ceramic materials accelerates the

degradation process, with the PCL bone bricks exhibiting the lowest weight reduction at day 5 (5.07%) and PCL/bioglass the highest weight loss (90%) followed by PCL/HA (81.41%) and PCL/TCP (10.85%). In the case of rectangular scaffolds, the results show that PCL/bioglass samples also degrade faster than their PCL/HA and PCL/TCP counterparts. Moreover, it was possible to observe that the increase in pore size accelerated the degradation process. The PCL/bioglass scaffolds with a 200 μm pore size were fully degraded after day 4, while the scaffolds with 300 μm and 500 μm pore sizes degraded after day 3. For PCL/HA, the results show that all samples (200 μm , 300 μm and 500 μm) were fully degraded after day 4. In the case of the PCL/TCP scaffolds, which were not fully degraded after day 5, the weight loss increased from 24.45% for scaffolds with a 200 μm pore size to 35.25% for scaffolds with a 500 μm pore size. A similar trend was observed for the PCL scaffolds (showing an 11.64% weight loss at day 5 for scaffolds with a 200 μm pore size and a 13.37% weight loss at day 5 for scaffolds with a 500 μm pore size), which exhibited the lowest degradation kinetics. This can be explained by the increase in the surface area exposed to the NaOH that accelerates the hydrolytic degradation and the release into the liquid medium of the ceramic particles previously bonded with the polymeric material [51–58]. Results also indicate that, for the same material composition, bone bricks degrade slower compared with rectangular scaffolds. As the overall porosity of the bone bricks is 52%, while the porosity of the rectangular scaffolds varies between 42% (scaffolds with a 200 μm pore size) and 56% (scaffolds with a 500 μm pore size), the observed differences can be attributed to the pore size gradient created in the bone bricks, which superimposes both the porosity and overall pore size (with an average of 350 μm in the bone bricks).

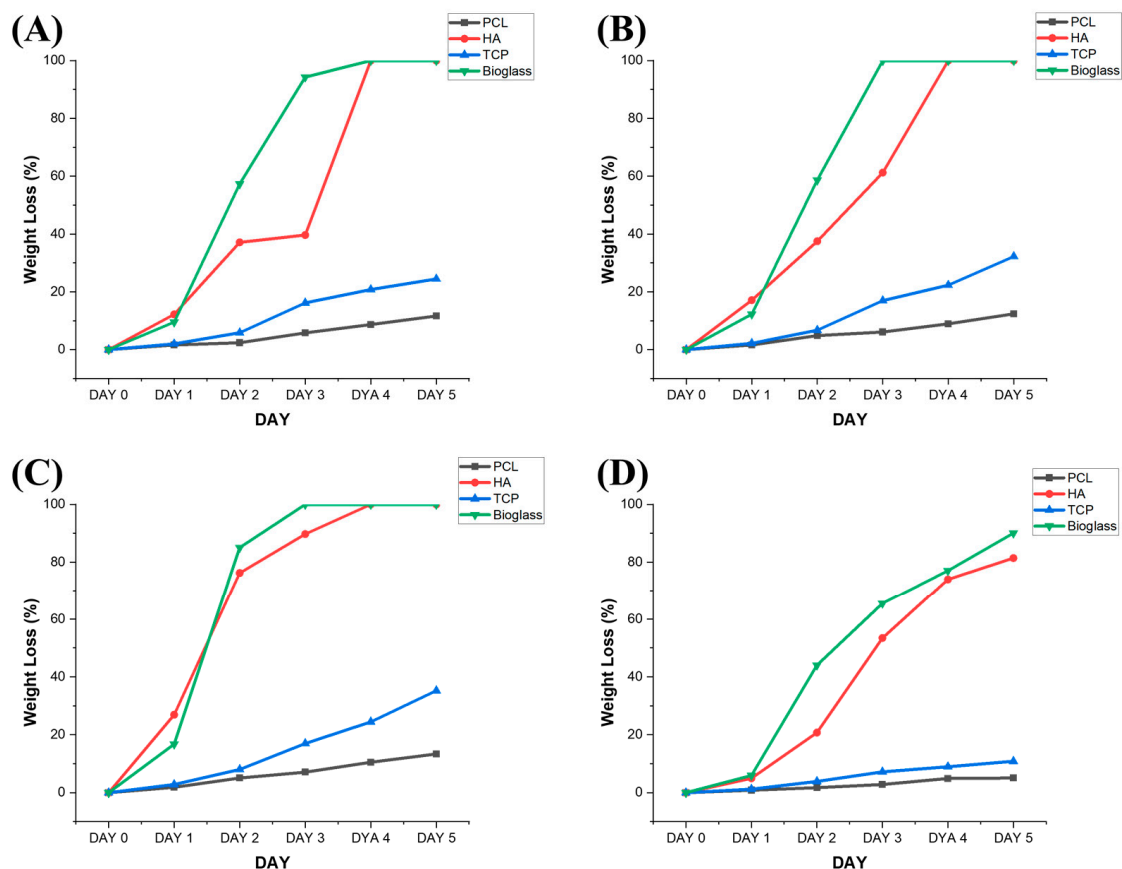


Figure 2. Weight loss as a function of degradation time for different samples and material compositions. (A) 200 μm pore size rectangular scaffolds, (B) 300 μm pore size rectangular scaffolds, (C) 500 μm pore size rectangular scaffolds and (D) bone bricks.

The effects of the scaffold architecture and material composition on the degradation kinetics can also be observed in Figures S1–S15 showing SEM images that, for the different

scaffolds and degradation time points, illustrate the surface erosion, decrease in the filament diameter and consequent increase in pore size, and filament collapse. Furthermore, from Tables 1–4 it is possible to observe that both pore size and porosity increase during the 5 days of degradation.

Table 1. Pore size and porosity values of bone brick scaffolds before and after the degradation process.

| Materials | Pore Size (μm) | Porosity (%) |
|--------------|-----------------------------|--------------|
| Day 0 | | |
| PCL | 333 \pm 90 | 52 |
| HA | 336 \pm 10 | 54 |
| TCP | 377 \pm 64 | 55 |
| Bioglass | 389 \pm 47 | 56 |
| Day 1 | | |
| PCL | 400 \pm 56 | 58 |
| HA | 398 \pm 31 | 58 |
| TCP | 412 \pm 94 | 60 |
| Bioglass | 430 \pm 29 | 62 |
| Day 2 | | |
| PCL | 402 \pm 63 | 58 |
| HA | 400 \pm 31 | 58 |
| TCP | 420 \pm 61 | 61 |
| Bioglass | 599 \pm 81 | 70 |
| Day 3 | | |
| PCL | 428 \pm 77 | 62 |
| HA | 657 \pm 52 | 75 |
| TCP | 443 \pm 26 | 64 |
| Bioglass | 678 \pm 41 | 77 |
| Day 4 | | |
| PCL | 452 \pm 42 | 65 |
| HA | 851 \pm 69 | 84 |
| TCP | 463 \pm 52 | 66 |
| Bioglass | 876 \pm 42 | 86 |
| Day 5 | | |
| PCL | 479 \pm 36 | 67 |
| HA | 505 \pm 8 | 90 |
| TCP | 510 \pm 47 | 69 |
| Bioglass | 616 \pm 6 | 92 |

Table 2. Pore size and porosity values of scaffolds (200 μm pore size) before and after the degradation process.

| Materials | Pore Size (μm) | Porosity (%) |
|--------------|-----------------------------|--------------|
| Day 0 | | |
| PCL | 205 \pm 1 | 42 |
| HA | 207 \pm 4 | 42 |
| TCP | 214 \pm 3 | 43 |
| Bioglass | 217 \pm 8 | 43 |

Table 2. *Cont.*

| Materials | Pore Size (μm) | Porosity (%) |
|--------------|-----------------------------|--------------|
| Day 1 | | |
| PCL | 214 \pm 5 | 43 |
| HA | 252 \pm 3 | 45 |
| TCP | 220 \pm 4 | 43 |
| Bioglass | 233 \pm 4 | 44 |
| Day 2 | | |
| PCL | 246 \pm 2 | 45 |
| HA | 443 \pm 53 | 64 |
| TCP | 249 \pm 1 | 45 |
| Bioglass | 333 \pm 15 | 52 |
| Day 3 | | |
| PCL | 249 \pm 2 | 45 |
| HA | 505 \pm 18 | 68 |
| TCP | 263 \pm 4 | 46 |
| Bioglass | 0 | 100 |
| Day 4 | | |
| PCL | 257 \pm 2 | 45 |
| HA | 0 | 100 |
| TCP | 281 \pm 6 | 47 |
| Bioglass | 0 | 100 |
| Day 5 | | |
| PCL | 257 \pm 2 | 45 |
| HA | 0 | 100 |
| TCP | 281 \pm 6 | 47 |
| Bioglass | 0 | 100 |

Table 3. Pore size and porosity values of scaffolds (300 μm pore size) before and after the degradation process.

| Materials | Pore Size (μm) | Porosity (%) |
|--------------|-----------------------------|--------------|
| Day 0 | | |
| PCL | 306 \pm 3 | 50 |
| HA | 310 \pm 5 | 50 |
| TCP | 312 \pm 3 | 50 |
| Bioglass | 315 \pm 7 | 51 |
| Day 1 | | |
| PCL | 314 \pm 3 | 50 |
| HA | 394 \pm 1 | 57 |
| TCP | 312 \pm 3 | 50 |
| Bioglass | 315 \pm 7 | 50 |
| Day 2 | | |
| PCL | 331 \pm 2 | 51 |
| HA | 420 \pm 3 | 61 |
| TCP | 345 \pm 1 | 53 |
| Bioglass | 462 \pm 4 | 66 |

Table 3. *Cont.*

| Materials | Pore Size (μm) | Porosity (%) |
|--------------|-----------------------------|--------------|
| Day 3 | | |
| PCL | 340 \pm 3 | 52 |
| HA | 630 \pm 7 | 73 |
| TCP | 354 \pm 1 | 53 |
| Bioglass | 0 | 100 |
| Day 4 | | |
| PCL | 345 \pm 2 | 53 |
| HA | 0 | 100 |
| TCP | 363 \pm 3 | 54 |
| Bioglass | 0 | 100 |
| Day 5 | | |
| PCL | 360 \pm 2 | 54 |
| HA | 0 | 100 |
| TCP | 364 \pm 1 | 54 |
| Bioglass | 0 | 100 |

Table 4. Pore size and porosity values of scaffolds (500 μm pore size) before and after the degradation process.

| Materials | Pore Size (μm) | Porosity (%) |
|--------------|-----------------------------|--------------|
| Day 0 | | |
| PCL | 502 \pm 3 | 68 |
| HA | 506 \pm 4 | 68 |
| TCP | 510 \pm 2 | 68 |
| Bioglass | 508 \pm 4 | 68 |
| Day 1 | | |
| PCL | 508 \pm 5 | 68 |
| HA | 608 \pm 1 | 70 |
| TCP | 515 \pm 6 | 68 |
| Bioglass | 544 \pm 3 | 69 |
| Day 2 | | |
| PCL | 538 \pm 6 | 68 |
| HA | 616 \pm 5 | 70 |
| TCP | 552 \pm 4 | 69 |
| Bioglass | 617 \pm 4 | 70 |
| Day 3 | | |
| PCL | 550 \pm 5 | 69 |
| HA | 837 \pm 4 | 84 |
| TCP | 561 \pm 5 | 69 |
| Bioglass | 0 | 100 |
| Day 4 | | |
| PCL | 556 \pm 6 | 69 |
| HA | 0 | 100 |
| TCP | 570 \pm 7 | 70 |
| Bioglass | 0 | 100 |
| Day 5 | | |
| PCL | 568 \pm 8 | 69 |
| HA | 0 | 100 |
| TCP | 583 \pm 1 | 70 |
| Bioglass | 0 | 100 |

3.2. Thermal Gravimetric Analysis

The thermal gravimetric analysis (TGA) results show that all considered samples exhibit degradation temperatures between 304.12 °C and 437.11 °C, after which only the inorganic materials remain (Figures S16 and S17). Moreover, the addition of ceramic particles into the polymer matrix reduces the degradation temperature, which can be observed for all samples throughout the degradation period. Moreover, the results in Table 5 and Figures S16 and S17 show that the overall weight ratio between polymer and ceramic material remains almost constant, while the total amount of ceramic materials significantly decreases, indicating a significant loss of polymer. For example, at day 3, the amount of HA in the samples is 22.4 wt%, and the total amount of HA is 9.4% of the initial HA content, while for the PCL/bioglass samples, the amount of bioglass in the samples is 22.1 wt%, and the total amount of bioglass is 7.1% of the initial bioglass content. These results clearly show a significant loss of polymer in the case of bioglass and confirm the observations discussed in Section 3.2 suggesting that the addition of ceramic materials (bioglass in particular) accelerates the degradation process. Additionally, this behaviour can also be explained by the morphological changes in the polymeric matrix, as discussed in Section 3.2.

Table 5. Designed and printed concentrations of PCL, HA, TCP and bioglass on the bone bricks and corresponding variations at different degradation time points.

| Bone Bricks | Designed Concentration of Inorganic Material (wt%) | Measured Concentration of Inorganic Material (wt%) | Inorganic Material that Remained (wt%) | Degradation Temperature (°C) |
|--------------|--|--|--|------------------------------|
| Day 0 | | | | |
| PCL | 0 | 0 | 0 | 437.11 ± 0.21 |
| HA | 20 | 20.27 ± 0.001 | 100 | 425.55 ± 0.38 |
| TCP | 20 | 20.38 ± 0.05 | 100 | 424.04 ± 0.23 |
| Bioglass | 20 | 20.68 ± 0.05 | 100 | 412.67 ± 0.18 |
| Day 1 | | | | |
| PCL | - | 0 | 0 | 436.95 ± 1.07 |
| HA | - | 21.64 ± 0.54 | 19.26 | 392.71 ± 1.42 |
| TCP | - | 19.45 ± 0.43 | 20.14 | 414.27 ± 0.18 |
| Bioglass | - | 20.73 ± 0.04 | 19.45 | 343.03 ± 0.12 |
| Day 2 | | | | |
| PCL | - | 0 | 0 | 435.79 ± 4.43 |
| HA | - | 20.77 ± 0.71 | 16.08 | 389.37 ± 2.51 |
| TCP | - | 19.41 ± 0.41 | 19.59 | 413.97 ± 0.86 |
| Bioglass | - | 21.71 ± 0.32 | 11.57 | 325.56 ± 2.26 |
| Day 3 | | | | |
| PCL | - | 0 | 0 | 431.83 ± 2.67 |
| HA | - | 22.44 ± 1.4 | 9.44 | 381.22 ± 2.63 |
| TCP | - | 18.92 ± 0.44 | 18.92 | 411.85 ± 0.12 |
| Bioglass | - | 22.14 ± 0.76 | 7.14 | 317.15 ± 2.16 |
| Day 4 | | | | |
| PCL | - | 0 | 0 | 431.83 ± 2.67 |
| HA | - | 21.11 ± 0.55 | 5.27 | 372.81 ± 1.64 |
| TCP | - | 18.69 ± 0.14 | 18.55 | 410.1 ± 1.21 |
| Bioglass | - | 18.12 ± 0.01 | 4.75 | 312.83 ± 3.41 |
| Day 5 | | | | |
| PCL | - | 0 | 0 | 427.87 ± 0.13 |
| HA | - | 21.34 ± 0.04 | 3.77 | 367.33 ± 9.5 |
| TCP | - | 18.17 ± 0.22 | 18.17 | 409.93 ± 0.01 |
| Bioglass | - | 19.14 ± 0.25 | 2.01 | 304.12 ± 5.78 |

As samples were printed at 90 °C, the results show that the printing conditions do not induce any material degradation. Additionally, the levels of HA, TCP and bioglass

determined with TGA (Table 1) suggest that the melt blending approach used to prepare the blends is a simple and efficient method.

3.3. Chemical Analysis

DSC was used to investigate the crystallinity (X_c), melting temperature (T_m), enthalpy (ΔH_m) and glass transition temperature (T_g) of bone bricks and rectangular scaffolds during the degradation process (Table 6 and Figure S18). The results show that the addition of ceramic materials into the polymer reduces the crystallinity (from 86.91% to 61.08%), the enthalpy (from 89.89 J/g to 65.06 J/g) and the melting temperature (from 64.65 °C to 69.82 °C), while the glass transition temperature slightly increases (from −59.19 °C to −59.1 °C) [58–63]. Similar results showing that the addition of ceramic particles constrains the crystallization process, limiting the mobility of PCL chains in the polymer–ceramic matrix and inducing the formation of smaller or thinner regions of crystalline lamellae, were also reported by other groups [64–67].

Table 6. Key thermal properties and crystallinity values for all samples at different degradation time points.

| Material | Day | T_g (°C) | T_m (°C) | ΔH_m (J/g) | χ_c (%) |
|----------|-------|------------|------------|--------------------|--------------|
| PCL | Day 0 | −59.19 | 64.65 | 89.89 | 86.91 |
| | Day 1 | −58.09 | 61.48 | 83.92 | 81.13 |
| | Day 2 | −58.03 | 60.83 | 81.23 | 78.54 |
| | Day 3 | −57.64 | 60.29 | 80.69 | 78.02 |
| | Day 4 | −55.81 | 55.06 | 79.2 | 76.58 |
| | Day 5 | −54.46 | 54.85 | 74.67 | 72.2 |
| HA | Day 0 | −59.22 | 60.98 | 65.06 | 61.08 |
| | Day 1 | −57.76 | 59.19 | 64.98 | 61.86 |
| | Day 2 | −56.74 | 58.85 | 64.98 | 51.98 |
| | Day 3 | −57 | 58 | 64.21 | 55.12 |
| | Day 4 | −56.45 | 57.63 | 63.92 | 15.94 |
| | Day 5 | 0 | 0 | 0 | 0 |
| TCP | Day 0 | −59.11 | 59.82 | 66.28 | 64.08 |
| | Day 1 | −58.58 | 59.73 | 66.16 | 63.96 |
| | Day 2 | −56.64 | 58.03 | 65.64 | 62.97 |
| | Day 3 | −58.57 | 57.8 | 64.58 | 60.82 |
| | Day 4 | −58.47 | 57.53 | 65.32 | 60.53 |
| | Day 5 | −58.41 | 57.42 | 65.22 | 59.37 |
| Bioglass | Day 0 | −59.1 | 59.94 | 68.48 | 66.21 |
| | Day 1 | −58.36 | 59.27 | 67.97 | 65.72 |
| | Day 2 | −57.82 | 57.33 | 64.34 | 48.4 |
| | Day 3 | −57.78 | 57.2 | 64.03 | 34.51 |
| | Day 4 | −57.69 | 56.01 | 63.91 | 25.76 |
| | Day 5 | −59.1 | 0 | 0 | 0 |

The results show that the melting temperature reduced for all the material compositions from day 0 to day 5, with the highest reduction observed for the bioglass scaffolds (there were no significant differences between PCL/bioglass and PCL/HA) and the lowest for TCP scaffolds. This can be explained by the decrease in crystallinity (with the highest reduction in the case of the PCL/HA and PCL/bioglass samples), and the melting temperature can be interpreted as the energy required by a system to destroy ordered regions. The results also show that the degradation occurs mainly through the destruction of the crystalline regions, which is aligned with the variations in both enthalpy and glass transition temperature that decrease and increase during the degradation time, respectively.

3.4. Mechanical Analysis

The compressive modulus results for all considered samples at different degradation time points are indicated in Figure 3. As observed, at day 0 and for the same material

composition, the printed bone scaffolds exhibited higher compressive moduli than their rectangular scaffold counterparts, indicating the relevance of the scaffold architecture on the mechanical performance. In the case of the rectangular scaffolds, the results show that for the same material composition, scaffolds with large pore sizes (500 μm) present lower compressive moduli than scaffolds with the lowest pore sizes (200 μm), which can be attributed to the increase in porosity. Furthermore, throughout the degradation process it can be observed that for bone bricks, the PCL/bioglass bone bricks present higher compressive moduli, while for rectangular scaffolds, the PCL/TCP scaffolds present higher compressive properties for all the different pore sizes. Moreover, compressive moduli decreased for all samples throughout the degradation process, which is associated with the decrease in crystallinity, decrease in the filament diameters, increase in porosity, filament collapse and limited adhesion between filaments.

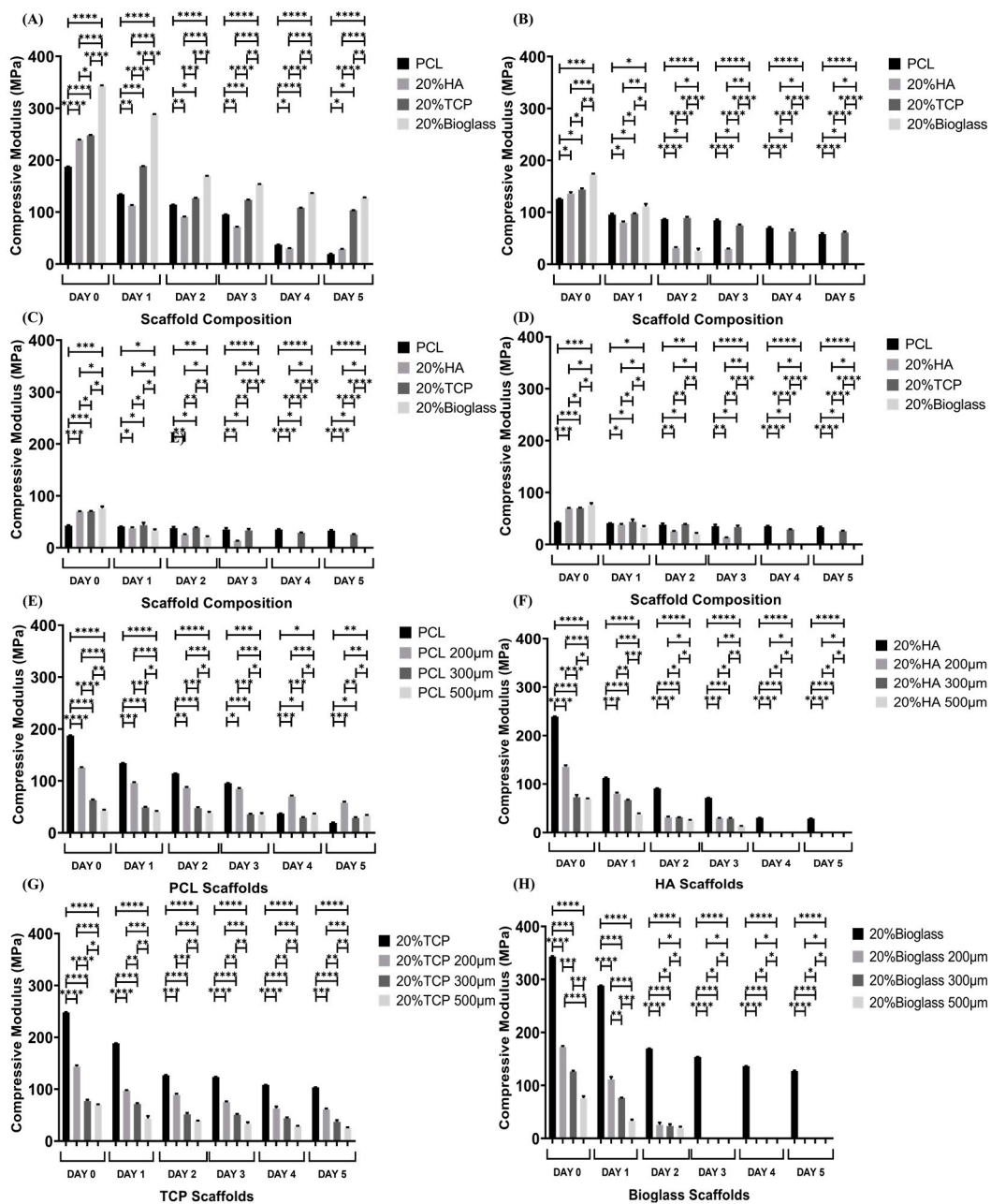


Figure 3. Compressive modulus as a function of degradation time for different architectures and material compositions. (A) Bone bricks scaffolds; (B) rectangular scaffolds with 200 μm pore size;

(C) rectangular scaffolds with 300 μm pore size; (D) rectangular scaffolds with 500 μm pore size; (E) PCL bone bricks and rectangular scaffolds; (F) HA bone bricks and rectangular scaffolds; (G) TCP bone bricks and rectangular scaffolds; and (H) bioglass bone bricks and rectangular scaffolds. * Statistical evidence ($p < 0.05$) analysed by one-way ANOVA, and Tukey post hoc test. The * statistical evidence ($p < 0.05$), **, *** and **** is the one-way analysis of variance (one-way ANOVA) and Tukey's post hoc test with the use of GraphPad Prism software and is used to show the difference between the results. The * is a small difference, while more * are added as the differences between the results increases.

4. Conclusions

The degradation kinetics of anatomically designed scaffolds with pore size gradients (bone bricks) and rectangular scaffolds with different pore sizes, considering a range of material compositions, was investigated, taking into consideration weight loss and morphological, thermal, chemical and mechanical changes. Due to the long degradation time of PCL, accelerated degradation, using NaOH, was considered. The results show that bone bricks present faster and more controlled degradation in comparison with rectangular scaffolds. The fastest degradation (weight loss) was observed for PCL/bioglass bone bricks and rectangular scaffolds. Moreover, for the same material composition, the degradation is faster in scaffolds presenting large pore sizes. The TGA results show that, in all considered cases, the concentration of the inorganic material remained the same during the degradation process. The DSC results indicate that the crystallinity of all samples at different degradation times decreased, suggesting a faster destruction of the crystalline regions than the amorphous ones. This observation is contrary to other studies suggesting that the degradation of PCL occurs through an initial mass loss that occurs due to the random hydrolytic split of polymeric chains in the amorphous regions, followed by a gradual degradation in the crystalline regions [63–66]. High levels of crystalline regions on the surfaces of the printed filaments together with the penetration of the degradation medium promoting internal degradation may explain the obtained results. Finally, as expected, compressive moduli decreased throughout the degradation process. However, for the same material content and degradation time point, bone bricks present better mechanical properties than rectangular scaffolds. Moreover, for the same material composition, better mechanical properties were observed for scaffolds with lower pore sizes. Overall, the accelerated degradation process showed that PCL/bioglass bone brick scaffolds present faster and more controlled degradation kinetics, compared with the other material concentrations and scaffold designs, and higher mechanical properties, making it the most suitable physical support for bone tissue applications.

Supplementary Materials: The following supporting information can be downloaded at: <https://www.mdpi.com/article/10.3390/polym15030670/s1>, Figure S1. Top and cross section images of PCL bone bricks at different degradation time points. (A,B) Day 1; (C,D) Day 2; (E,F), Day 3; (G,H) Day 4; (I,J) Day 5; Figure S2. Top and cross section images of PCL/HA bone bricks at different degradation time points. (A,B) Day 1; (C,D) Day 2; (E,F), Day 3; (G,H) Day 4; (I,J) Day 5; Figure S3. Top and cross section images of PCL/TCP bone bricks at different degradation time points. (A,B) Day 1; (C,D) Day 2; (E,F), Day 3; (G,H) Day 4; (I,J) Day 5; Figure S4. Top and cross section images of PCL/bioglass bone bricks at different degradation time points. (A,B) Day 1; (C,D) Day 2; (E,F), Day 3; (G,H) Day 4; (I) Day 5; Figure S5. Top and cross section images of PCL rectangular scaffolds with 200 μm of pore size at different degradation time points. (A,B) Day 1; (C,D) Day 2; (E,F) Day 3; (G,H) Day 4; (I,J) Day 5; Figure S6. Top and cross section images of PCL rectangular scaffolds with 300 μm of pore size at different degradation time points. (A,B) Day 1; (C,D) Day 2; (E,F) Day 3; (G,H) Day 4; (I,J) Day 5; Figure S7. Top and cross section images of PCL rectangular scaffolds with 500 μm of pore size at different degradation time points. (A,B) Day 1; (C,D) Day 2; (E,F) Day 3; (G,H) Day 4; (I,J) Day 5; Figure S8. Top and cross section images of PCL/HA rectangular scaffolds with 200 μm of pore size at different degradation time points. (A,B) Day 1; (C,D) Day 2; (E) Day 3; Figure S9. Top and cross section images of PCL/HA rectangular scaffolds with 300 μm of pore size at different degradation time points. (A,B) Day 1; (C,D) Day 2; (E) Day 3; Figure S10. Top and cross section images of PCL/HA

rectangular scaffolds with 500 μm of pore size at different degradation time points. (A,B) Day 1; (C,D) Day 2; Figure S11. Top and cross section images of PCL/TCP rectangular scaffolds with 200 μm of pore size at different degradation time points. (A,B) Day 1; (C,D) Day 2; (E,F) Day 3; (G,H) Day 4; (I,J) Day 5; Figure S12. Top and cross section images of PCL/TCP rectangular scaffolds with 300 μm of pore size at different degradation time points. (A,B) Day 1; (C,D) Day 2; (E,F) Day 3; (G,H) Day 4; (I,J) Day 5; Figure S13. Top and cross section images of PCL/TCP rectangular scaffolds with 500 μm of pore size at different degradation time points. (A,B) Day 1; (C,D) Day 2; (E,F) Day 3; (G,H) Day 4; (I,J) Day 5; Figure S14. Top and cross section images of PCL/bioglass rectangular scaffolds with 200 μm of pore size at different degradation time points. (A,B) Day 1; (C,D) Day 2; Figure S15. Top and cross section images of PCL/bioglass rectangular scaffolds with 300 μm of pore size at different degradation time points. (A,B) Day 1; (C) Day 2; Figure S16. Thermal Gravimetric Analysis (TGA) curves of bone bricks at different degradation times. (A) Day 1, (B) Day 2, (C) Day 3, (D) Day 4 and (E) Day 5; Figure S17. Thermal Gravimetric Analysis (TGA) curves of bone bricks samples as a function of degradation time for different material compositions. (A) PCL, (B) PCL/HA, (C) PCL/TCP and (D) PCL/bioglass; Figure S18. Glass transition temperature and heating curves for bone bricks containing different material composition as a function of degradation time. (A) Glass transition temperature on day 0, (B) Heating curve on day 0, (C) Glass transition temperature on day 1, (D) Heating curve on day 1, (E) Glass transition temperature on day 2 and (F) Heating curve on day 2, (G) Glass transition temperature on day 3, (H) Heating curve on day 3, (I) Glass transition temperature on day 4, (J) Heating curve on day 4, (K) Glass transition temperature on day 5 and (L) Heating curve on day 5.

Author Contributions: Conceptualization, E.D. and P.B.; methodology, E.D., M.H.H., A.M.O., A.A.A. and A.F.; software, E.D. and A.F.; validation, E.D., M.H.H., A.M.O., A.A.A., A.F. and P.B.; formal analysis, E.D. and P.B.; investigation, E.D., M.H.H., A.M.O., A.F. and P.B.; resources, all authors.; data curation, all authors; writing—original draft preparation, E.D.; writing—review and editing, all authors; visualization, E.D. and P.B.; supervision, G.C., A.W., G.B., B.K. and P.B.; project administration, P.B.; funding acquisition, P.B. All authors have read and agreed to the published version of the manuscript.

Funding: This project was supported by the University of Manchester and the Engineering and Physical Sciences Research Council (EPSRC) of the U.K. and the Global Challenges Research Fund (GCRF), grant number EP/R01513/1.

Data Availability Statement: Not applicable.

Acknowledgments: The authors would like to thank the support received from both the University of Manchester and the Engineering and Physical Sciences Research Council (EPSRC) of the U.K. This manuscript is the result of the work completed by Evangelos Daskalakis toward a Ph.D. in Mechanical Engineering, granted by the University of Manchester in September of 2022.

Conflicts of Interest: The authors declare no conflict of interest.

References

1. Bruyas, A.; Lou, F.; Stahl, A.; Gardner, M.; Maloney, W.; Goodman, S.; Yang, Y. Systematic characterization of 3D-printed PCL/ β -TCP scaffolds for biomedical devices and bone tissue engineering: Influence of composition and porosity. *J. Mater. Res.* **2018**, *33*, 1948–1959. [[CrossRef](#)]
2. Chlanda, A.; Kijeńska-Gawrońska, E.; Zdunek, J.; Swieszkowski, W. Internal nanocrystalline structure and stiffness alterations of electrospun polycaprolactone-based mats after six months of in vitro degradation. An atomic force microscopy assay. *J. Mech. Behav. Biomed. Mater.* **2020**, *101*, 103437. [[CrossRef](#)] [[PubMed](#)]
3. Díaz, E.; Aresti, J.; León, J. Evaluation of physicochemical and mechanical properties with the in vitro degradation of PCL/nHA/MWCNT composite scaffolds. *J. Reinf. Plast. Compos.* **2020**, *40*, 134–142. [[CrossRef](#)]
4. Pogorielov, M.; Hapchenko, A.; Deineka, V.; Rogulska, L.; Oleshko, O.; Vodsed'álková, K.; Berezkinová, L.; Vysloužilová, L.; Klápšťová, A.; Erben, J. In vitro degradation and in vivotoxicity of NanoMatrix3D[®] polycaprolactone and poly(lactic acid) nanofibrous scaffolds. *J. Biomed. Mater. Res. Part A* **2018**, *106*, 2200–2212. [[CrossRef](#)] [[PubMed](#)]
5. Melnik, E.; Shkarina, S.; Ivlev, S.; Weinhardt, V.; Baumbach, T.; Chaikina, M.; Surmeneva, M.; Surmenev, R. In vitro degradation behaviour of hybrid electrospun scaffolds of polycaprolactone and strontium-containing hydroxyapatite microparticles. *Polym. Degrad. Stab.* **2019**, *167*, 21–32. [[CrossRef](#)]
6. Motealleh, A.; Eqtesadi, S.; Pajares, A.; Miranda, P. Enhancing the mechanical and in vitro performance of robocast bioglass scaffolds by polymeric coatings: Effect of polymer composition. *J. Mech. Behav. Biomed. Mater.* **2018**, *84*, 35–45. [[CrossRef](#)]

7. Conoscenti, G.; Carfi Pavia, F.; Ciraldo, F.; Liverani, L.; Brucato, V.; La Carrubba, V.; Boccaccini, A. In vitro degradation and bioactivity of composite poly-L-lactic (PLLA)/bioactive glass (BG) scaffolds: Comparison of 45S5 and 1393BG compositions. *J. Mater. Sci.* **2017**, *53*, 2362–2374. [[CrossRef](#)]
8. Gaikwad, A.; Lu, W.; Dey, S.; Bhattarai, P.; Chia, C.; Larby, J.; Haug, G.; Myers, S.; Jaffar, J.; Westall, G.; et al. Vascular remodelling in IPF patients and its detrimental effect on lung physiology: Potential role of endothelial to mesenchymal transition (EndMT). *ERJ Open Res.* **2022**, *8*, 00571-2021. [[CrossRef](#)]
9. Mousovich-Neto, F.; Matos, M.; Costa, A.; Melo Reis, R.; Atella, G.; Miranda-Alves, L.; Carvalho, D.; Ketzer, L.; Corrêa da Costa, V. Brown adipose tissue remodelling induced by corticosterone in male Wistar rats. *Exp. Physiol.* **2019**, *104*, 514–528. [[CrossRef](#)]
10. Wang, G.; Mohammadtursun, N.; Lv, Y.; Zhang, H.; Sun, J.; Dong, J. Baicalin Exerts Anti-Airway Inflammation and Anti-Remodelling Effects in Severe Stage Rat Model of Chronic Obstructive Pulmonary Disease. *Evid.-Based Complement. Altern. Med.* **2018**, *2018*, 7591348. [[CrossRef](#)]
11. Rijsbergen, M.; van Rietbergen, B.; Barthelemy, V.; Eltes, P.; Lazáry, Á.; Lacroix, D.; Noailly, J.; Ho Ba Tho, M.; Wilson, W.; Ito, K. Comparison of patient-specific computational models vs. clinical follow-up, for adjacent segment disc degeneration and bone remodelling after spinal fusion. *PLoS ONE* **2018**, *13*, e0200899. [[CrossRef](#)]
12. Wong, S.; Tamatam, C.; Cho, I.; Toth, P.; Bargi, R.; Belvitch, P.; Lee, J.; Rehman, J.; Reddy, S.; Shin, J. Inhibition of aberrant tissue remodelling by mesenchymal stromal cells singly coated with soft gels presenting defined chemomechanical cues. *Nat. Biomed. Eng.* **2021**, *6*, 54–66. [[CrossRef](#)] [[PubMed](#)]
13. Contessotto, P.; Pandit, A. Therapies to prevent post-infarction remodelling: From repair to regeneration. *Biomaterials* **2021**, *275*, 120906. [[CrossRef](#)]
14. Kubota, S.I.; Takahashi, K.; Mano, T.; Matsumoto, K.; Katsumata, T.; Shi, S.; Tainaka, K.; Ueda, H.R.; Ehata, S.; Miyazono, K. Whole-organ analysis of TGF- β -mediated remodelling of the tumour microenvironment by tissue clearing. *Commun. Biol.* **2021**, *4*, 294. [[CrossRef](#)] [[PubMed](#)]
15. Maes, L.; Cloet, A.S.; Fourneau, I.; Famaey, N. A homogenized constrained mixture model of restenosis and vascular remodelling after balloon angioplasty. *J. R. Soc. Interface* **2021**, *18*, 20210068. [[CrossRef](#)] [[PubMed](#)]
16. Żóttowska, S.; Koltsov, I.; Alejski, K.; Ehrlich, H.; Ciałkowski, M.; Jesionowski, T. Thermal decomposition behaviour and numerical fitting for the pyrolysis kinetics of 3D spongin-based scaffolds. The classic approach. *Polym. Test.* **2021**, *97*, 107148. [[CrossRef](#)]
17. He, Y.; Santana, M.; Staneviciute, A.; Pimentel, M.; Yang, F.; Goes, J.; Kawaji, K.; Vaicik, M.; Abdulhadi, R.; Hibino, N.; et al. Hydrogel Scaffolds: Cell-Laden Gradient Hydrogel Scaffolds for Neovascularization of Engineered Tissues (Adv. Healthcare Mater. 7/2021). *Adv. Healthcare Mater.* **2021**, *10*, 2170030. [[CrossRef](#)]
18. Bose, S.; Bhattacharjee, A.; Banerjee, D.; Boccaccini, A.; Bandyopadhyay, A. Influence of random and designed porosities on 3D printed tricalcium phosphate-bioactive glass scaffolds. *Addit. Manuf.* **2021**, *40*, 101895. [[CrossRef](#)]
19. González-Pérez, F.; Ibáñez-Fonseca, A.; Alonso, M.; Rodríguez-Cabello, J. Combining tunable proteolytic sequences and a VEGF-mimetic peptide for the spatiotemporal control of angiogenesis within Elastin-Like Recombinamer scaffolds. *Acta Biomater.* **2021**, *130*, 149–160. [[CrossRef](#)]
20. Fernandes, J.; Soek, R.; do Nascimento, T.; Menezes, L.; Sasaki, G.; Campos, R. Degradation of Organophosphates Promoted by 1,2,4-Triazole Anion: Exploring Scaffolds for Efficient Catalytic Systems. *J. Org. Chem.* **2021**, *86*, 4027–4034. [[CrossRef](#)]
21. Bartnikowski, M.; Abdal-hay, A.; Bartnikowski, N.; Kyoung Kim, Y.; Ivanovski, S. A comprehensive study of acid and base treatment of 3D printed poly(ϵ -caprolactone) scaffolds to tailor surface characteristics. *Appl. Surf. Sci.* **2021**, *555*, 149602. [[CrossRef](#)]
22. Dong, Q.; Zhang, M.; Zhou, X.; Shao, Y.; Li, J.; Wang, L.; Chu, C.; Xue, F.; Yao, Q.; Bai, J. 3D-printed Mg-incorporated PCL-based scaffolds: A promising approach for bone healing. *Mater. Sci. Eng. C.* **2021**, *129*, 112372. [[CrossRef](#)] [[PubMed](#)]
23. Gao, J.; Chen, S.; Tang, D.; Jiang, L.; Shi, J.; Wang, S. Mechanical Properties and Degradability of Electrospun PCL/PLGA Blended Scaffolds as Vascular Grafts. *Trans. Tianjin Univ.* **2018**, *25*, 152–160. [[CrossRef](#)]
24. Sánchez-González, S.; Diban, N.; Urtiaga, A. Hydrolytic Degradation and Mechanical Stability of Poly(ϵ -caprolactone)/Reduced Graphene Oxide Membranes as Scaffolds for In Vitro Neural Tissue Regeneration. *Membranes* **2018**, *8*, 12. [[CrossRef](#)] [[PubMed](#)]
25. Woodard, L.; Grunlan, M. Hydrolytic Degradation of PCL–PLLA Semi-IPNs Exhibiting Rapid, Tunable Degradation. *ACS Biomater. Sci. Eng.* **2018**, *5*, 498–508. [[CrossRef](#)] [[PubMed](#)]
26. Woodard, L.; Grunlan, M. Hydrolytic Degradation and Erosion of Polyester Biomaterials. *ACS Macro Lett.* **2018**, *7*, 976–982. [[CrossRef](#)]
27. Farzan, A.; Borandeh, S.; Zanjanzadeh Ezazi, N.; Lipponen, S.; Santos, H.; Seppälä, J. 3D scaffolding of fast photocurable polyurethane for soft tissue engineering by stereolithography: Influence of materials and geometry on growth of fibroblast cells. *Eur. Polym. J.* **2020**, *139*, 109988. [[CrossRef](#)]
28. Silva, M.; Ferreira, F.N.; Alves, N.M.; Paiva, M.C. Biodegradable polymer nanocomposites for ligament/tendon tissue engineering. *J. Nanobiotechnol.* **2020**, *18*, 23. [[CrossRef](#)] [[PubMed](#)]
29. Liu, X.; Hou, P.; Liu, S.; Qi, J.; Feng, S.; Zhang, L.; Ma, P.; Bai, W. Effect of poly(lactic-co-glycolic acid) blend ratios on the hydrolytic degradation of poly(*para*-dioxanone). *J. Polym. Res.* **2021**, *28*, 166. [[CrossRef](#)]
30. Anju, S.; Prajitha, N.; Sukanya, V.; Mohanan, P. Complicity of degradable polymers in health-care applications. *Mater. Today Chem.* **2020**, *16*, 100236. [[CrossRef](#)]

31. Ben Abdallah, A.; Kallel, A.; Gamaoun, F.; Tcharkhtchi, A. Enzymatic Hydrolysis of Poly (Caprolactone) and its Blend with Styrene–Butadiene–Styrene (40% PCL/60% SBS). *J. Polym. Environ.* **2019**, *27*, 2341–2351. [[CrossRef](#)]
32. Leroux, A.; Ngoc Nguyen, T.; Rangel, A.; Cacciapuoti, I.; Duprez, D.; Castner, D.; Migonney, V. Long-term hydrolytic degradation study of polycaprolactone films and fibers grafted with poly(sodium styrene sulfonate): Mechanism study and cell response. *Biointerphases* **2020**, *15*, 061006. [[CrossRef](#)] [[PubMed](#)]
33. Germain, L.; Fuentes, C.; van Vuure, A.; des Rieux, A.; Dupont-Gillain, C. 3D-printed biodegradable gyroid scaffolds for tissue engineering applications. *Mater. Des.* **2018**, *151*, 113–122. [[CrossRef](#)]
34. Prabhath, A.; Vernekar, V.; Vasu, V.; Badon, M.; Avochinou, J.; Asandei, A.; Kumbar, S.; Weber, E.; Laurencin, C. Kinetic degradation and biocompatibility evaluation of polycaprolactone-based biologics delivery matrices for regenerative engineering of the rotator cuff. *J. Biomed. Mater. Res. Part A* **2021**, *109*, 2137–2153. [[CrossRef](#)] [[PubMed](#)]
35. Reddy, M.; Ponnamma, D.; Choudhary, R.; Sadasivuni, K. A Comparative Review of Natural and Synthetic Biopolymer Composite Scaffolds. *Polymers* **2021**, *13*, 1105. [[CrossRef](#)]
36. Erdal, N.; Lando, G.; Yadav, A.; Srivastava, R.; Hakkarainen, M. Hydrolytic Degradation of Porous Crosslinked Poly(ϵ -Caprolactone) Synthesized by High Internal Phase Emulsion Templating. *Polymers* **2020**, *12*, 1849. [[CrossRef](#)]
37. Sattary, M.; Khorasani, M.; Rafienia, M.; Rozve, H. Incorporation of nanohydroxyapatite and vitamin D3 into electrospun PCL/Gelatin scaffolds: The influence on the physical and chemical properties and cell behavior for bone tissue engineering. *Polym. Adv. Technol.* **2017**, *29*, 451–462. [[CrossRef](#)]
38. Ogueri, K.; Jafari, T.; Escobar Ivirico, J.; Laurencin, C. Polymeric Biomaterials for Scaffold-Based Bone Regenerative Engineering. *Regener. Eng. Transl. Med.* **2018**, *5*, 128–154. [[CrossRef](#)] [[PubMed](#)]
39. Saudi, A.; Zebarjad, S.; Salehi, H.; Katouezadeh, E.; Alizadeh, A. Assessing physicochemical, mechanical, and in vitro biological properties of polycaprolactone/poly(glycerol sebacate)/hydroxyapatite composite scaffold for nerve tissue engineering. *Mater. Chem. Phys.* **2022**, *275*, 125224. [[CrossRef](#)]
40. Li, R.; Song, Y.; Fouladian, P.; Arafat, M.; Chung, R.; Kohlhagen, J.; Garg, S. Three-Dimensional Printing of Curcumin-Loaded Biodegradable and Flexible Scaffold for Intracranial Therapy of Glioblastoma Multiforme. *Pharmaceutics* **2021**, *13*, 471. [[CrossRef](#)]
41. Bazgir, M.; Zhang, W.; Zhang, X.; Elies, J.; Saeinasab, M.; Coates, P.; Youseffi, M.; Sefat, F. Degradation and Characterisation of Electrospun Polycaprolactone (PCL) and Poly(lactic-co-glycolic acid) (PLGA) Scaffolds for Vascular Tissue Engineering. *Materials* **2021**, *14*, 4773. [[CrossRef](#)] [[PubMed](#)]
42. Wang, Y.; Huang, H.; Jia, G.; Zeng, H.; Yuan, G. Fatigue and dynamic biodegradation behavior of additively manufactured Mg scaffolds. *Acta Biomater.* **2021**, *135*, 705–722. [[CrossRef](#)] [[PubMed](#)]
43. Saranti, A.; Tiron-Stathopoulos, A.; Papaioannou, L.; Gioti, C.; Ioannou, A.; Karakassides, M.; Avgoustakis, K.; Koutselas, I.; Dimos, K. 3D-printed bioactive scaffolds for bone regeneration bearing carbon dots for bioimaging purposes. *Smart Mater. Med.* **2022**, *3*, 12–19. [[CrossRef](#)]
44. He, J.; Lin, Z.; Hu, X.; Xing, L.; Liang, G.; Chen, D.; An, J.; Xiong, C.; Zhang, X.; Zhang, L. Biocompatible and biodegradable scaffold based on poly(trimethylene carbonate-tricalcium phosphate) microspheres for tissue engineering. *Colloids Surf. B Biointerfaces* **2021**, *204*, 111808. [[CrossRef](#)]
45. Kleer-Reiter, N.; Julmi, S.; Feichtner, F.; Waselau, A.; Klose, C.; Wriggers, P.; Maier, H.; Meyer-Lindenberg, A. Biocompatibility and degradation of the open-pored magnesium scaffolds LAE442 and La2. *Biomed. Mater.* **2021**, *16*, 035037. [[CrossRef](#)]
46. Krieghoff, J.; Kascholke, C.; Loth, R.; Starke, A.; Koenig, A.; Schulz-Siegmund, M.; Hacker, M. Composition-controlled degradation behavior of macroporous scaffolds from three-armed biodegradable macromers. *Polym. Degrad. Stab.* **2022**, *195*, 109775. [[CrossRef](#)]
47. Kowalewicz, K.; Vorndran, E.; Feichtner, F.; Waselau, A.; Brueckner, M.; Meyer-Lindenberg, A. In-Vivo Degradation Behavior and Osseointegration of 3D Powder-Printed Calcium Magnesium Phosphate Cement Scaffolds. *Materials* **2021**, *14*, 946. [[CrossRef](#)]
48. Daskalakis, E.; Huang, B.; Vyas, C.; Acar, A.; Liu, F.; Fallah, A.; Cooper, G.; Weightman, A.; Blunn, G.; Koç, B.; et al. Bone Bricks: The Effect of Architecture and Material Composition on the Mechanical and Biological Performance of Bone Scaffolds. *ACS Omega* **2022**, *7*, 7515–7530. [[CrossRef](#)]
49. Daskalakis, E.; Huang, B.; Vyas, C.; Acar, A.; Fallah, A.; Cooper, G.; Weightman, A.; Koc, B.; Blunn, G.; Bartolo, P. Novel 3D Bioglass Scaffolds for Bone Tissue Regeneration. *Polymers* **2022**, *14*, 445. [[CrossRef](#)]
50. Huang, B.; Wang, Y.; Vyas, C.; Bartolo, P. Crystal Growth of 3D Poly(ϵ -caprolactone) Based Bone Scaffolds and Its Effects on the Physical Properties and Cellular Interactions. *Adv. Sci.* **2022**, *10*, 2203183. [[CrossRef](#)]
51. Guo, L.; Du, Z.; Wang, Y.; Cai, Q.; Yang, X. Degradation behaviors of three-dimensional hydroxyapatite fibrous scaffolds stabilized by different biodegradable polymers. *Ceram. Int.* **2020**, *46*, 14124–14133. [[CrossRef](#)]
52. Tarik Arafat, M.; Lam, C.; Ekaputra, A.; Wong, S.; He, C.; Hutmacher, D.; Li, X.; Gibson, I. High performance additive manufactured scaffolds for bone tissue engineering application. *Soft Matter* **2011**, *7*, 8013. [[CrossRef](#)]
53. Lam, C.; Hutmacher, D.; Schantz, J.; Woodruff, M.; Teoh, S. Evaluation of polycaprolactone scaffold degradation for 6 months in vitro and in vivo. *J. Biomed. Mater. Res. Part A* **2009**, *90A*, 906–919. [[CrossRef](#)] [[PubMed](#)]
54. Dong, Y.; Suryani, L.; Zhou, X.; Muthukumaran, P.; Rakshit, M.; Yang, F.; Wen, F.; Hassanbhai, A.; Parida, K.; Simon, D.; et al. Synergistic Effect of PVDF-Coated PCL-TCP Scaffolds and Pulsed Electromagnetic Field on Osteogenesis. *Int. J. Mol. Sci.* **2021**, *22*, 6438. [[CrossRef](#)] [[PubMed](#)]
55. Lam, C.; Savalani, M.; Teoh, S.; Hutmacher, D. Dynamics of in vitro polymer degradation of polycaprolactone-based scaffolds: Accelerated versus simulated physiological conditions. *Biomed. Mater.* **2008**, *3*, 034108. [[CrossRef](#)]

56. Siqueira, D.; Luna, C.; Araújo, E.; Barros, A.; Wellen, R. Approaches on PCL/macaíba biocomposites—Mechanical, thermal, morphological properties and crystallization kinetics. *Polym. Adv. Technol.* **2021**, *32*, 3572–3587. [[CrossRef](#)]
57. Przybysz-Romatowska, M.; Barczewski, M.; Mania, S.; Tercjak, A.; Haponiuk, J.; Formela, K. Morphology, Thermo-Mechanical Properties and Biodegradability of PCL/PLA Blends Reactively Compatibilized by Different Organic Peroxides. *Materials* **2021**, *14*, 4205. [[CrossRef](#)]
58. Lam, C.; Teoh, S.; Hutmacher, D. Comparison of the degradation of polycaprolactone and polycaprolactone-(β -tricalcium phosphate) scaffolds in alkaline medium. *Polym. Int.* **2007**, *56*, 718–728. [[CrossRef](#)]
59. Salerno, A.; Domingo, C. Pore structure properties of scaffolds constituted by aggregated microparticles of PCL and PCL-HA processed by phase separation. *J. Porous Mater.* **2015**, *22*, 425–435. [[CrossRef](#)]
60. Zhang, B.; Wang, L.; Song, P.; Pei, X.; Sun, H.; Wu, L.; Zhou, C.; Wang, K.; Fan, Y.; Zhang, X. 3D printed bone tissue regenerative PLA/HA scaffolds with comprehensive performance optimizations. *Mater. Des.* **2021**, *201*, 109490. [[CrossRef](#)]
61. Luo, K.; Wang, L.; Wang, Y.; Zhou, S.; Zhang, P.; Li, J. Porous 3D hydroxyapatite/polyurethane composite scaffold for bone tissue engineering and its in vitro degradation behavior. *Ferroelectrics* **2020**, *566*, 104–115. [[CrossRef](#)]
62. Fanovich, M.A.; Ivanovic, J.; Zizovic, I.; Misic, D.; Jaeger, P. Functionalization of polycaprolactone/hydroxyapatite scaffolds with *Usnea lethariiformis* extract by using supercritical CO₂. *Mater. Sci. Eng. C* **2016**, *58*, 204–212. [[CrossRef](#)] [[PubMed](#)]
63. Dziadek, M.; Pawlik, J.; Menaszek, E.; Stodolak-Zych, E.; Cholewa-Kowalska, K. Effect of the preparation methods on architecture, crystallinity, hydrolytic degradation, bioactivity, and biocompatibility of PCL/bioglass composite scaffolds. *J. Biomed. Mater. Res. Part B Appl. Biomater.* **2014**, *103*, 1580–1593. [[CrossRef](#)]
64. Wang, Z.; Lim, J.; Ho, Y.; Zhang, Q.; Chong, M.; Tang, M.; Hong, M.; Chan, J.; Teoh, S.; Thian, E. Biomimetic three-dimensional anisotropic geometries by uniaxial stretching of poly(ϵ -caprolactone) films: Degradation and mesenchymal stem cell responses. *J. Biomed. Mater. Res. Part A* **2013**, *102*, 2197–2207. [[CrossRef](#)]
65. Zhang, Q.; Jiang, Y.; Zhang, Y.; Ye, Z.; Tan, W.; Lang, M. Effect of porosity on long-term degradation of poly(ϵ -caprolactone) scaffolds and their cellular response. *Polym. Degrad. Stab.* **2013**, *98*, 209–218. [[CrossRef](#)]
66. Kirillova, A.; Yeazel, T.; Asheghali, D.; Petersen, S.; Dort, S.; Gall, K.; Becker, M. Fabrication of Biomedical Scaffolds Using Biodegradable Polymers. *Chem. Rev.* **2021**, *121*, 11238–11304. [[CrossRef](#)] [[PubMed](#)]
67. Hajebi, S.; Mohammadi Nasr, S.; Rabiee, N.; Bagherzadeh, M.; Ahmadi, S.; Rabiee, M.; Tahriri, M.; Tayebi, L.; Hamblin, M. Bioresorbable composite polymeric materials for tissue engineering applications. *Int. J. Polym. Mater. Polym. Biomater.* **2020**, *70*, 926–940. [[CrossRef](#)]

Disclaimer/Publisher’s Note: The statements, opinions and data contained in all publications are solely those of the individual author(s) and contributor(s) and not of MDPI and/or the editor(s). MDPI and/or the editor(s) disclaim responsibility for any injury to people or property resulting from any ideas, methods, instructions or products referred to in the content.